AIP Journal of Applied Physics

Factors affecting the f×Q product of 3C-SiC microstrings: What is the upper limit for sensitivity?

Atieh R. Kermany, James S. Bennett, George A. Brawley, Warwick P. Bowen, and Francesca Iacopi

Citation: Journal of Applied Physics **119**, 055304 (2016); doi: 10.1063/1.4941274
View online: http://dx.doi.org/10.1063/1.4941274
View Table of Contents: http://scitation.aip.org/content/aip/journal/jap/119/5?ver=pdfcov
Published by the AIP Publishing

JOURNAL OF APPLIED PHYSICS **119**, 055304 (2016)

Factors affecting the $f \times Q$ product of 3C-SiC microstrings: What is the upper limit for sensitivity?

Atieh R. Kermany,[1] James S. Bennett,[2] George A. Brawley,[2] Warwick P. Bowen,[2] and Francesca Iacopi[1,a)]
[1]*Queensland Micro- and Nanotechnology Centre, Griffith University, Nathan, QLD 4111, Australia*
[2]*School of Mathematics and Physics, The University of Queensland, St. Lucia, QLD 4072, Australia*

(Received 17 November 2015; accepted 21 January 2016; published online 2 February 2016)

The $f_n \times Q$ (Hz) is a crucial sensitivity parameter for micro-electro-mechanical sensing. We have recently shown a $f_n \times Q$ product of $\sim 10^{12}$ Hz for microstrings made of cubic silicon carbide on silicon, establishing a new state-of-the-art and opening new frontiers for mass sensing applications. In this work, we analyse the main parameters influencing the frequency and quality factor of silicon carbide microstrings (material properties, microstring geometry, clamping condition, and environmental pressure) and investigate the potential for approaching the theoretical upper limit. We indicate that our previous result is only about a factor 2 lower than the thermoelastic dissipation limit. For fully reaching this upper limit, a substantial reduction of the defects in the silicon carbide thin film would be required, while maintaining a high residual tensile stress in the perfect-clamped strings. © *2016 AIP Publishing LLC*. [http://dx.doi.org/10.1063/1.4941274]

I. INTRODUCTION

Resonant microbeam sensors consist of a beam structure vibrating at its resonance, with or without a sensing layer coated on the surface. These sensors have high reliability, sensitivity, selectivity, and performance due to their quasi-digital frequency output signal and small size.[1,2]

In addition, resonant sensors made of thin films are compatible with integrated chip (IC)-process technology which facilitates the integration and batch production of miniaturized, low-power, and low-cost devices.[3,4]

The most common use of resonant microbeam sensors has been for mass detection.[5,6] These resonators function as accurate mass sensors because their frequency (fn) shifts when an additional mass is adsorbed on their surface (Fig. 1).[7,8] Howe and Muller were first to demonstrate a resonant mass sensor for vapors detection in 1986.[9] Numerous developments have been achieved since, and currently detection of single DNA molecule,[10] single cell,[11] single virus,[12] and single protein[7] masses are possible.

The sensitivity of microbeam mass sensors can be enhanced by reducing their effective mass (m_{eff}), and increasing their f_n and quality factor (Q).[13] Although shrinking the resonator size can help increasing the f_n[14] and improving the sensitivity to external disturbances, it negatively affects the resonator Q[15–17] and the total adsorption area. Therefore, a trade-off is present between the total absorption area and the maintaining or improving of the high f_n and high Q to improve the sensor sensitivity, resolution, and accuracy.[18,19] Consequently, two key figures of merit of $f_n \times Q$ (Hz) and $R \times Q$ (nm^{-1}), where R is the resonator's surface-to-volume ratio, are used to evaluate the sensor performance.[17,20]

To enhance the Q, it is important to select the appropriate microbeam clamping type. Cantilever (single-clamped beam) resonators generally result in higher quality factor due to the reduced clamping losses compared to strings or bridges (double-clamped beam).[21,22] However, the converse is true when the material carries residual strain, as is the case for SiC-on-Si microbeams.[23,24] Material selection is also crucial in order to achieve high f_n values as the frequency is directly proportional to the material properties. Silicon carbide (SiC) is a wide bandgap semiconductor with outstanding electrical, chemical, and mechanical properties, which makes it an excellent material for high frequency applications.[25–36] Among its polytypes, cubic SiC (3C-SiC) is widely used for MEMS applications as it can be deposited epitaxially on silicon, allowing large areas to be easily micromachined at low cost.[29,37] In addition, the lattice and thermal expansion mismatches between Si and SiC result in the formation of defects and residual stress within the epitaxial SiC film.[37–39] We have previously shown that we could achieve $f_n \times Q$ product of $\sim 10^{12}$ (Hz) with large absorption area through the application of cubic silicon carbide (3C-SiC) microstrings with high intrinsic tensile mean stress, which outperforms the highest reported state of the art silicon nitride (a-Si_3N_4) microstrings and offer high promise for chemical sensing.[29]

In this work, we explore the factors affecting the $R \times Q$ and $f_n \times Q$ products of the fundamental out-of-plane flexural mode of 3C-SiC microstrings, including the film quality, residual mean stress (σ), geometry, clamping condition, and environmental pressure. In the light of the theory and our experimental data, we will offer guidelines for obtaining the maximum sensitivity for 3C-SiC microstrings.

This paper is divided into five sections. Section II includes the description of the parameters that impact the f_n and Q. Section III explains the fabrication steps. Section IV includes the results and discussion, followed by the conclusion (Section V).

a)Author to whom correspondence should be addressed. Electronic mail: f.iacopi@griffith.edu.au

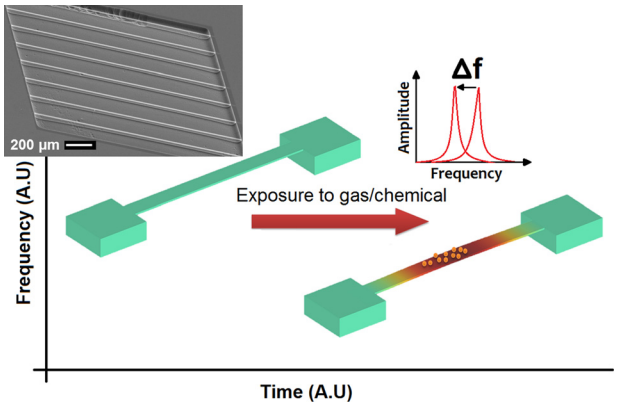

FIG. 1. Schematic of the mass detection mechanism of a microstring, vibrating at its out-of-plane fundamental flexural mode; the inset is a scanning electron microscope (SEM) image of an array of fabricated strings.

II. MECHANICAL PERFORMANCE OF FLEXURAL MICROSTRINGS

The mechanical frequency in hetero-epitaxial flexural strings is influenced by the string geometry, mode number, and material properties according to the strain-dependent correction of the Euler-Bernoulli theory[40–43]

$$f_n = \frac{\kappa_n}{4\pi\sqrt{3}}\sqrt{\frac{E}{\rho}}\frac{t}{l^2}\sqrt{1+\gamma_n\frac{\sigma l^2}{Et^2}}, \tag{1}$$

where n is the mode number, κ_n the eigen-value ($\kappa_n = (n+1/2)\pi$), γ_n is a mode-dependent coefficient ($\gamma_n = 12(\kappa_n - 2)/\kappa_n^3$), l is the string length, t is the string thickness, ρ is the density, and E is the Young's modulus. If the width (w) of the beam is large compared to its thickness (t), such that $(w) \geq 5t$, it is necessary to replace E with $E(1-\nu^2)^{-1}$, with ν being Poisson's ratio.

At the same time, Q is inversely proportional to the external losses (Q_{ext}^{-1}), such as viscous damping and clamping loss,[44] and internal damping (Q_{int}^{-1}) as shown in Equation (2).[45] Internal damping includes the thermoelastic, volume, and surface losses[40]

$$Q^{-1} = \sum Q_{ext}^{-1} + \sum Q_{\text{int}}^{-1}. \tag{2}$$

When operating in vacuum, the viscous damping from the environment can be eliminated.[44,46] This makes the clamping (i.e., anchor or support) loss[22] the dominant dissipation factor for microstrings operating in high vacuum. Internal damping including surface, volume, and thermoelastic damping[40] generally becomes important after minimizing or eliminating the external sources of dissipation, including clamping losses.[44]

Since the thermoelastic dissipation sets the upper limit to the $f_n \times Q$ product of microstring resonators, it is useful to calculate the thermoelastic Q (Q_{TED}) for the bending dominated resonators theoretically as indicated by Lifshitz and Roukes[47]

$$Q_{TED} = \frac{c_v}{ET\alpha^2}\left(\frac{6}{\xi^2} - \frac{6}{\xi^3}\frac{\sinh\xi + \sin\xi}{\cosh\xi + \cos\xi}\right)^{-1}, \tag{3}$$

$$\text{with } \xi = t\sqrt{\frac{2\pi f_n c_v}{2\kappa}}, \tag{4}$$

where T is the temperature, c_v is the specific heat capacity constant volume, α is the thermal expansion coefficient, and κ is the thermal conductivity. This theoretical expression makes it possible to determine how closely a given string is operating to the thermoelastic limit.

A. Clamping loss in flexural beams

Clamping loss is the result of energy propagation from the vibrating structure clamping points into the substrate.[48] Jimbo and Itao were first to report the effects of cantilever geometry on clamping loss (Q_{Clamp}^{-1}) in 1968.[49] Later in 2001, Cross and Lifshitz[50] confirmed the geometry dependency of Q_{Clamp}^{-1} using a two-dimensional model for both the out-of-plane and the in-plane movements as shown in Equations (5) and (6), respectively,

$$\text{Out-of-plane}: Q_{Clamp}^{-1} \propto \frac{w}{l}, \tag{5}$$

$$\text{In-plane}: Q_{Clamp}^{-1} \propto \frac{w^3}{l^3}. \tag{6}$$

After that, Photiadis and Judge[51] calculated the clamping loss using 3-dimesional models where support thickness is also considered. Their equation can be approximated to Equation (5) for the standard out-of-plane perfect-clamped beams. Other works have also reported similar dependencies.[52,53] Meanwhile, Schmid and Hierold[54] reported that in the case of string resonators, the influence of width on Equation (5) is negligible.

In addition, Verbridge *et al.*[23] reported that the microstrings Q_{Clamp}^{-1} reduces through the application of a tensile mean stress. This influence is also confirmed by other literature[29,55–58] including our recent work as shown in Table I.

B. Review of the influence of tensile stress

In addition to increasing the f_n (Equation (1)), tensile stress is also reported to significantly improve the Q of MEMS and nano-electro-mechanical (NEMS) strings by reducing the energy dissipation through the anchors.[27] A residual mean stress can be applied to the bridge/string material intrinsically through the deposition and growth process,[16,29,57,59] or extrinsically through the bending of the substrate chip,[58,60] the application of an electrostatic force, and stiction.[61] Table I shows the summary of some of the literature data on the enhancement of strings and bridges f_n and Q through the application of a tensile stress and in vacuum. Intrinsic tensile stress is applied to nos. 1–4 and 6 of Table I. Note that unlike a-Si_3N_4, the mean stress in strings fabricated from SiC and gallium arsenide (GaAs) can be tuned in a controlled manner through hetero-epitaxial growth, by changing the Si substrate orientation and the epitaxial sacrificial layer, respectively. Finally, the tensile stress is applied to no. 8 in Table I using chip-bending method. We can learn from the table that the tensile stress indeed improves both f_n and Q for strings regardless of material properties. We note

TABLE I. Summary of the mechanical behavior of the strings/bridges in the literature.

No.	Material	P (mbar)	l-w-t (μm)-(μm)-(nm)	σ (MPa)	f_n (kHz)	Q	$f_n \times Q$ (Hz)	$R \times Q$ (nm^{-1})	Q_{TED}
1	a-Si_3N_4[52,53]	10^{-5}	1553-4-177	190	78.7	2×10^6	1.6×10^{11}	23601	1.1×10^8
2	a-Si_3N_4[53]	10^{-5}	1553-4-157	890	176	3×10^6	5.3×10^{11}	39720	6.2×10^7
3	SiC(111)[28]	2×10^{-7}	1000-4-255	750	220	8×10^5	1.8×10^{11}	6843	7.2×10^6
4	SiC(111)[28]	10^{-6}	930-4-255	1500	280.5	3×10^6	$\mathbf{8.4 \times 10^{11}}$	25035	5.6×10^6
5	GaAs[54]	…	37-10-200	Unstrained	1230	1800	2.2×10^9	18	…
6	GaAs[54]	…	53-10-200	35% along the beam	2900	2×10^3	5.5×10^{10}	194	…
7	Al[55]	$<10^{-3}$	5-3-10	Unstrained	…	…	9.5×10^8	…	…
8	Al[55]	$<10^{-3}$	5-3-10	13.5	…	…	1.9×10^9	…	…

that the SiC(111) intrinsic tensile stress can be tuned to be as high as 1500 MPa.

III. EXPERIMENT

3C-SiC films were deposited hetero-epitaxially on 150 mm Si wafers at 1000 °C in a hot-wall horizontal low-pressure chemical vapour deposition system, using silane (SiH_4) and propene (C_3H_6) gases.[62] A Veeco Wyko NT1100 optical profilometer with a 1 Å resolution was applied to measure the thickness using a refractive index of 2.65 for 3C-SiC films.[63] We measured E values of 400 GPa and 330 GPa for SiC(111) and SiC(100), respectively, using Hysitron Triboindenter nanoindentation on 1 μm thick films.[64] These values are in agreement with the data reported in literature.[27,40] The residual mean stresses were measured with a Tencor Flexus 2320 curvature measurement system and throughout SiC film etch-back process in nm resolution as explained in our previous work.[65] We measured SiC(111) mean stresses of 650 MPa and 230 MPa for the film thicknesses of 255 nm and 50 nm, respectively. Similarly, we measured a mean stress of 250 MPa for a film thickness of 255 nm of SiC(100), which is evidently much smaller than the SiC(111) wafer of similar thickness. In addition, we measured the SiC films root-mean-square (RMS) roughness to be ~3 nm using Park NX20 atomic force microscopy (AFM) in non-contact mode.[66]

We fabricated a range of epitaxial 3C-SiC microstrings deposited on on-axis Si(100) and Si(111) with lengths of up to 2600 μm, thicknesses of 50 nm and 255 nm, and widths of 4–12 μm through the four stages of photolithography, SiC anisotropic etching using hydrogen chloride (HCl), Si isotropic etching using xenon difluoride (XeF_2), and photoresist removal through TEGAL 915 oxygen plasma. We applied two lithography stages, as explained in our previous work,[29] in order to ensure that the strings are perfectly clamped. The first step was to pattern the SiC film prior to SiC etching and the second step was to cover the anchors before the Si etching to prevent them from being over-etched due to the isotropic behavior of the Si etching process. To further emphasize the importance of the quality of the string anchors on Q, we have also fabricated equivalent set perfect-clamped strings with intentional residues left behind on their clamping points, to be compared with strings with perfectly clean anchors.

We simulated the fundamental out-of-plane mode f_n of the strings using finite element modelling (FEM) IntelliSuite software (version 8.7). We used our measured E and residual gradient stress, the density of 3.21 g cm^{-3}, Poisson's ratio values of 0.267 and 0.235 for SiC(100) and SiC(111)[27,67] in the IntelliSuite software for the FEM analysis. The SiC stress was modelled by subdividing the 3C-SiC string into multiple layers with specific thicknesses according to our experimentally measured high resolution residual gradient stress profile.[65]

Measurement of the fundamental out-of-plane mode f_n and Q of the strings was made using all-fibre Mach-Zehnder optical interferometry. The interferometer[68] used a reflowed lensed fibre to focus 40 μW of 780 nm light from a low-noise CW laser (SOLSTIS TiS laser by M Squared) onto the sample, mounted on a micropositioning stage (SLC-24 by SmarAct GmbH). Reflected light was collected by the same fibre and detected using the balanced heterodyne method. Acousto-optic modulation was used to offset the local oscillator frequency from the probe frequency by 68.8 MHz. Signals were recorded with an N9010a Agilent signal analyser to obtain mechanical mode spectra. Next, the Q factors were obtained using the free ring-down method[69] with piezo-electric actuation.

All measurements were performed at room temperature, and under uniform high vacuum of 7.7×10^{-7} mbar. However, in order to establish the intrinsic and molecular pressure behaviour ranges for the fabricated SiC strings, a series of measurements were also performed at different levels of vacuum (Section IV C).

Finally, to estimate the sensor ultimate sensitivity and to check that how closely the sensor is operating to its upper limit, we calculated the Q_{TED} using T of 300 K, and SiC properties of c_v of 3×10^6 J/(m^3 K), α of 3×10^{-6} (K^{-1}), and κ of 70 W/(m K).[70]

IV. RESULTS AND DISCUSSION

We stated in our earlier work that both f_n and Q of microstrings are strongly affected by the residual tensile stress within the SiC film. We reported an $f_n \times Q$ product of up to 10^{12} (Hz) for a SiC(111) string with a length of 930 μm, width of 4 μm, and thickness of 255 nm. This string was subject to a residual mean tensile stress of 1500 MPa, one of the highest reported values of similar size devices (as shown in Table I).

To further understand the factors influencing the mechanical behavior of the strings, we measured the f_n and Q factors of SiC strings with different film qualities, lengths,

TABLE II. Measured mechanical behavior values for microstrings.

	…	l-w (μm)	2600-4					1000-4				
Material	σ (MPa)	t (nm)	f_n (kHz)	Q	$f_n \times Q$ (Hz)	$R \times Q$ (nm^{-1})	Q_{TED}	f_n (kHz)	Q	$f_n \times Q$ (Hz)	$R \times Q$ (nm^{-1})	Q_{TED}
SiC(111)	650	255	77	2.4×10^6	1.8×10^{11}	20025	2.1×10^7	202	5.5×10^5	1.1×10^{11}	4590	7.8×10^6
SiC(111)	230	50	42.1	2.6×10^5	1.1×10^{10}	10530	9.8×10^8	…	…	…	…	…
SiC(100)	250	255	45	1.6×10^6	7.2×10^{10}	13350	4.3×10^7	118	6×10^5	7.1×10^{10}	5007	1.6×10^7

widths, and thicknesses in high vacuum (7.7×10^{-7} mbar) as shown in Table II and also with different clamping and vacuum conditions as shown in Table III and Fig. 3. Thanks to the excellent fracture toughness and tensile strength of the SiC film,[71–73] we could fabricate the 3C-SiC strings as long as 2600 μm, as thin as 50 nm. The measured fundamental modes varied within a 10% window from the simulation results, confirming that the FEM model is reasonably accurate (the simulation is discussed in detail in our previous study[29]).

A. Material properties and string geometry

We can observe from Table II that the string f_n is directly proportional to $\sqrt{\sigma}$ for similar *l-w* geometries, the ratio of the f_n values are almost the same as the ratio of their $\sqrt{\sigma}$; $((f_{n1}/f_{n2}) \approx (\sqrt{\sigma_1}/\sqrt{\sigma_2}))$, because the influence of E and t can be neglected following Equation (1). Consequently, SiC(111) with 50 nm thickness and SiC(100) with 255 nm thickness have similar f_n values due to their similar mean stress values.

At the same time, from Table II we observe that for similar geometries and film thickness, SiC(111) and SiC(100) strings have comparable Q values even though the SiC(100) string has considerably lower mean stress (250 MPa) than SiC(111) strings (650 MPa). This is attributed to the film quality influence on the Q factor. The quality of thin heteroepitaxial SiC on silicon films is notoriously hindered by an extensive amount of crystal defects due to the large lattice mismatch of the system, and we reported previously that our SiC(100) films have an overall better crystal quality than SiC(111) films, thanks to a faster stress relaxation rate.[64,74] It is therefore expected that SiC(100) film would have a smaller component of defect-driven energy dissipation. Therefore, the effect of the mean stress is compensated by the influence of the film quality, resulting in the comparable Q factors.

In addition, the Q factor decreases by almost an order of magnitude (from 2.4×10^6 to 2.6×10^5) as the thickness reduces from 255 nm to 50 nm for the SiC(111) strings with the same *l-w* geometries. The reduction can be linked to the decrease of the mean stress from 650 MPa to 230 MPa and also the fact that the defect density[66] is very high for 50 nm thickness, as the initial few nanometers of heteroepitaxial growth is the most defective part of the film. This results in high energy dissipation in the 50 nm thick strings and so a substantially lower Q. The stress variation through the thickness, which is called the residual gradient stress, is the result of the stress relaxation through the film defects.[64,65]

Overall, the SiC(111) strings show higher values of $f_n \times Q$ and $R \times Q$ than the SiC(100) strings for the same thickness due to their higher mean stress value. Note though that in terms of Q factors alone, the SiC(100) strings could potentially perform as well as the SiC(111) bridges, thanks to their higher crystal quality. However, their substantially lower residual stress drastically limits their $f_n \times Q$ performance. Finally, we can observe that both $f_n \times Q$ and $R \times Q$ increase as the strings length increase, due to a substantial increase of Q, able to compensate for the reduction in natural resonating frequencies.

We can conclude from Tables I and II that SiC(111) with 1500 MPa mean stress has the closest Q-factor (3×10^6) to the thermoelastic limit Q_{TED} (5.6×10^6), calculated from Equation (3). We calculated the $f_n \times Q$ of this string to be 8.4×10^{11} Hz which is only about a factor 2 away from its upper limit ($f_n \times Q_{\mathrm{TED}}$: 1.6×10^{12} Hz). Overall, this indicates that in order to pursue the maximum sensitivity and to reach the potential theoretical limit, a reduction of the defects in the SiC thin film is ideally required. In parallel, increasing the string length and maximizing the residual tensile film stress effectively enhance the $f_n \times Q$ and $R \times Q$ products. Clearly, long strings under high tension will be more likely to fracture, and as such the improvement in defect density is a must.

TABLE III. Measured Q factors for microstrings without residues (Q_1) and with photoresist residues (Q_2) on their anchors. The values are an average out of five measurements.

l-w-t (μm)	Q_1	Q_2
2600-4-0.255	2.4×10^6	9×10^4
1000-4-0.255	5.5×10^5	2.7×10^4

B. String clamping condition

We reported previously that the Q of our microstrings is limited by clamping losses.[29] We showed that it is important to implement perfect-clamping[29] as the design of the perfect-clamped resonators helps to reduce the clamping loss and the coupling between the resonator and the surrounding environment.[48,55] To further analyse the effect of the clamping conditions on Q, we have fabricated and compared the resonant frequencies and corresponding Q factors of two equivalent sets of resonators made of SiC(111) with the dimensions mentioned in Table III. The first set was prepared with a non-optimal photoresist removal step, leaving intentionally behind photoresist residues around the string clamping points or anchors (Fig. 2(a)), which are the most difficult areas for photoresist stripping. On the second set, we used our

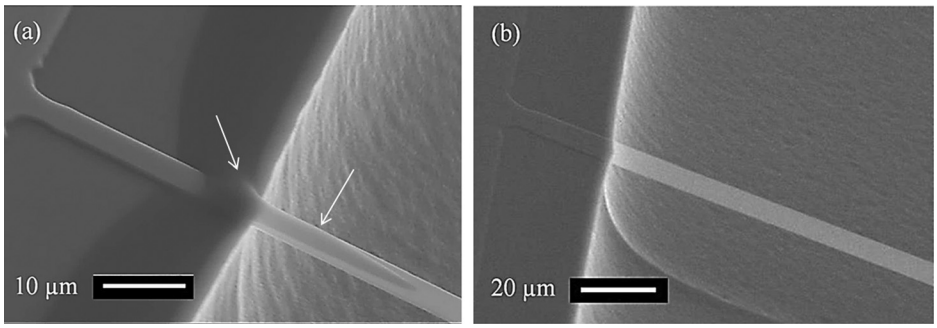

FIG. 2. SEM of a microstring with residual photoresist on its anchors (a), and a completely clean microstring (b), used for the comparison in Table III. The photoresist residues in (a) are highlighted by arrows.

optimized oxygen plasma process for resist removal, obtaining complete clearance of the photoresist from the strings, including their clamping points (Fig. 2(b)).

Our comparison indicated similar f_n values for both clamping conditions (with and without residues). However, we found that the Q decreased by more than one order of magnitude for the strings with photoresist residues on its anchors as shown in Table III.

C. Influence of environmental pressure

Viscous or air damping is the most significant source of dissipation in MEMS when not operating in vacuum.[44] Therefore, it is important to understand the Q dependency on pressure. In 1968, Newell[75] introduced different regions of pressure, namely, viscous, molecular (fine vacuum), and intrinsic (high vacuum) from ambient pressure to vacuum. Where, the Q is proportional to $1/P$ in molecular regime, and becomes independent of the pressure as P reduces and enters the intrinsic region.[76,77] In addition, the boundaries of the molecular region varies according to the device dimension.[16]

We analysed, the influence of the pressure on the Q for the high vacuum (7.7×10^{-7} mbar) through the low vacuum (4.4×10^{-2} mbar) conditions. We observed that the Q reduces from 1.0×10^6 to 4.1×10^3 as the pressure goes from high- towards low-vacuum levels due to the fluid damping. The dependency can be divided into two regimes as shown in Fig. 3.

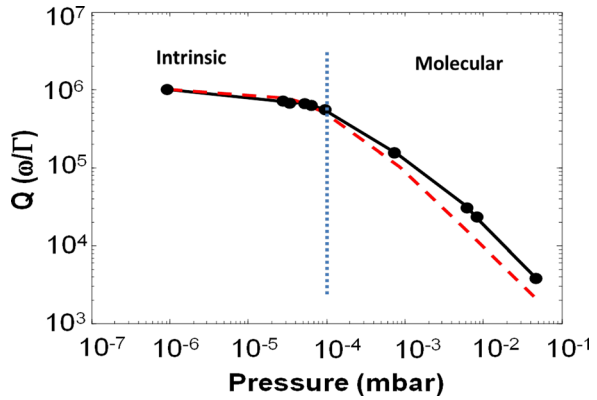

FIG. 3. Environmental pressure effect on the Q for a SiC(111) string with 2600 μm length, 4 μm width, and 50 nm thickness. The pressure varies from 7.7×10^{-7} mbar to 4.4×10^{-2} mbar with the Q reducing from 1.03×10^6 to 4.1×10^3. The dashed line is the fitted line, while the vertical line is added only to guide the eye.

We used the function $Q = 1/((1/Q_0) + \alpha^* P)$ for the fitting purpose (shown with a dashed line in Fig. 3), where Q_0 is the measured Q-factor of the intrinsic region (1.03×10^6) and α is a fitting factor (0.01017) calculated based on the measured Q–P values.

We can observe from Fig. 3 that for pressure values above 10^{-4} mbar, the αP factor dominates the Q_0 of the fitting function, resulting in a direct dependency between the Q and $1/P$, which means that the device is operating in the molecular region. However, for pressure values below 10^{-4} mbar, the dependency of Q on the pressure becomes milder and eventually negligible as pressure reduces because the Q_0 of the fitting function starts to dominate the αP factor, indicating an intrinsic pressure region.

From this study, we can conclude that a pressure of about 10^{-4} mbar represents the limit between the intrinsic and molecular regimes for the fabricated SiC strings. This also means that any pressure variation below 10^{-4} mbar will have only negligible effects on the Q factors, and Q factors measured at any pressure below this value can be compared with reasonable accuracy.

V. CONCLUSION

We have recently demonstrated $f_n \times Q$ products in the order of $\sim 10^{12}$ Hz using 3C-SiC thin film, the highest reported value for a microstring. Here, we have conducted an in-depth analysis of the parameters influencing the f_n and Q values of a 3C-SiC microstring in order to explore the potential of reaching the theoretical limit ($f_n \times Q_{TED}$) of sensitivity for mass sensing applications. Our analysis indicate that we are only a factor of 2 away from the ultimate sensitivity for 3C-SiC strings, and that an additional improvement is potentially achievable through the use of (1) high vacuum environment, (2) perfect-clamped anchors, clean from any residues, (3) high intrinsic SiC film residual tensile stress, (4) improved SiC crystalline quality, and (5) strings with tailored geometry, i.e., high length to width ratio. In particular, as long strings under high tension will be more likely to fracture, and as such the improvement in defect density is required.

In conclusion, we emphasize here that microstrings made of heteroepitaxial SiC on silicon outperform other thin film materials in terms of resonant performance. In addition, SiC offers the additional potential for maintaining such high Qs in the actual sensing device by using graphene directly grown on SiC film[35] as a conductor in the place of metal layers, one of the largest sources of damping in electromechanical resonators.

ACKNOWLEDGMENTS

Fabrication was performed using the equipment of the Australian National Fabrication Facilities (ANFF), Queensland node. We thank Neeraj Mishra for the experimental support. The authors acknowledge the support from AFOSR through the AOARD 15IOA053 grant and the Australian Research Council through the Discovery Project No. DP140100734. Associate Professor Francesca Iacopi and Associate Professor Warwick P. Bowen are the recipients of Australian Research Council Future Fellowship (FT120100445 and FT140100650, respectively).

[1]R. M. Langdon, J. Phys. E **18**(2), 103 (1985).
[2]G. Stemme, J. Micromech. Microeng. **1**(2), 113 (1991).
[3]H. Yu, P. Xu, X. Xia, D. W. Lee, and X. Li, IEEE Trans. Ind. Electron. **59**(12), 4881 (2012).
[4]M. Ahmed, M. Khawaja, M. Notarianni, B. Wang, D. Goding, B. Gupta, J. J. Boeckl, A. Takshi, N. Motta, and S. E. Saddow, Nanotechnology **26**(43), 434005 (2015).
[5]V. Cimalla, F. Niebelschütz, K. Tonisch, C. Foerster, K. Brueckner, I. Cimalla, T. Friedrich, J. Pezoldt, R. Stephan, and M. Hein, Sens. Actuators, B **126**(1), 24 (2007).
[6]P. S. Waggoner and H. G. Craighead, Lab Chip **7**(10), 1238 (2007).
[7]A. K. Naik, M. S. Hanay, W. K. Hiebert, X. L. Feng, and M. L. Roukes, Nat. Nanotechnol. **4**(7), 445 (2009).
[8]E. Buks and B. Yurke, Phys. Rev. E: Stat. Phys. Plasmas Fluids Relat. Interdiscip. Top. **74**(4), 046619 (2006).
[9]R. T. Howe and R. S. Muller, IEEE Trans. Electron Devices **33**(4), 499 (1986).
[10]B. Ilic, Y. Yang, K. Aubin, R. Reichenbach, S. Krylov, and H. G. Craighead, Nano Lett. **5**(5), 925 (2005).
[11]B. Ilic, D. Czaplewski, M. Zalalutdinov, H. G. Craighead, P. Neuzil, C. Campagnolo, and C. Batt, J. Vac. Sci. Technol., B **19**(6), 2825 (2001).
[12]A. Gupta, D. Akin, and R. Bashir, Appl. Phys. Lett. **84**(11), 1976 (2004).
[13]K. L. Ekinci, Y. T. Yang, and M. L. Roukes, J. Appl. Phys. **95**(5), 2682 (2004).
[14]X. M. H. Huang, C. A. Zorman, M. Mehregany, and M. L. Roukes, Nature **421**(6922), 496 (2003).
[15]C. M. Lin, Y. Y. Chen, V. V. Felmetsger, D. G. Senesky, and A. P. Pisano, Adv. Mater. **24**(20), 2722 (2012).
[16]S. S. Verbridge, H. G. Craighead, and J. M. Parpia, Appl. Phys. Lett. **92**(1), 013112 (2008).
[17]J. H. Ko, J. Jeong, J. Choi, and M. Cho, Appl. Phys. Lett. **98**(17), 171909 (2011).
[18]I. Bargatin, E. B. Myers, J. S. Aldridge, C. Marcoux, P. Brianceau, L. Duraffourg, E. Colinet, S. Hentz, P. Andreucci, and M. L. Roukes, Nano Lett. **12**(3), 1269 (2012).
[19]K. L. Ekinci and M. L. Roukes, Rev. Sci. Instrum. **76**(6), 061101 (2005).
[20]X. Liu, J. F. Vignola, H. J. Simpson, B. R. Lemon, B. H. Houston, and D. M. Photiadis, J. Appl. Phys. **97**(2), 023524 (2005).
[21]K. Jensen, K. Kim, and A. Zettl, Nat. Nanotechnol. **3**(9), 533 (2008).
[22]M. Imboden and P. Mohanty, Phys. Rep. **534**(3), 89 (2014).
[23]S. S. Verbridge, J. M. Parpia, R. B. Reichenbach, L. M. Bellan, and H. G. Craighead, J. Appl. Phys. **99**(12), 124304 (2006).
[24]S. Schmid, S. Dohn, and A. Boisen, Sensors **10**(9), 8092 (2010).
[25]N. G. Wright and A. B. Horsfall, Mater. Matters **4**, 5 (2009).
[26]M. Bhatnagar and B. J. Baliga, IEEE Trans. Electron Devices **40**(3), 645 (1993).
[27]V. Cimalla, J. Pezoldt, and O. Ambacher, J. Phys. D: Appl. Phys. **40**(20), 6386 (2007).
[28]C. A. Zorman and R. J. Parro, Phys. Status Solidi B **245**(7), 1404 (2008).
[29]A. R. Kermany, G. Brawley, N. Mishra, E. Sheridan, W. P. Bowen, and F. Iacopi, Appl. Phys. Lett. **104**(8), 081901 (2014).
[30]H. P. Phan, D. V. Dao, L. Wang, T. Dinh, N. T. Nguyen, A. Qamar, P. Tanner, S. Dimitrijev, and Y. Zhu, J. Mater. Chem. C **3**(6), 1172 (2015).
[31]N. G. Wright and A. B. Horsfall, J. Phys. D: Appl. Phys. **40**(20), 6345 (2007).
[32]Y. T. Yang, K. L. Ekinci, X. M. H. Huang, L. M. Schiavone, M. L. Roukes, C. A. Zorman, and M. Mehregany, Appl. Phys. Lett. **78**(2), 162 (2001).
[33]N. G. Wright, *Kirk-Othmer Encyclopedia of Chemical Technology* (Wiley, New York, 2006).
[34]J. M. Leger, J. Haines, and B. Blanzat, J. Mater. Res. Sci. Lett. **13**(23), 1688 (1994).
[35]B. V. Cunning, M. Ahmed, N. Mishra, A. R. Kermany, B. Wood, and F. Iacopi, Nanotechnology **25**(32), 325301 (2014).
[36]P. M. Sarro, Sens. Actuators, A **82**(1), 210 (2000).
[37]A. Severino, C. Locke, R. Anzalone, M. Camarda, N. Piluso, A. La Magna, S. Saddow, G. Abbondanza, G. D'Arrigo, and F. La Via, ECS Trans. **35**(6), 99 (2011).
[38]R. Anzalone, M. Camarda, C. Locke, D. Alquier, A. Severino, M. Italia, D. Rodilosso, C. Tringali, A. La Magna, and G. Foti, J. Electrochem. Soc. **157**(4), H438 (2010).
[39]M. Zielinski, J. F. Michaud, S. Jiao, T. Chassagne, A. E. Bazin, A. Michon, M. Portail, and D. Alquier, J. Appl. Phys. **111**, 053507 (2012).
[40]K. Brueckner, F. Niebelschuetz, K. Tonisch, C. Foerster, V. Cimalla, R. Stephan, J. Pezoldt, T. Stauden, O. Ambacher, and M. A. Hein, Phys. Status Solidi A **208**(2), 357 (2011).
[41]M. Wijesundara and R. Azevedo, *Silicon Carbide Microsystems for Harsh Environments* (Springer, 2011).
[42]M. Mehregany and C. A. Zorman, Thin Solid Films **355**, 518 (1999).
[43]R. G. Azevedo, D. G. Jones, A. V. Jog, B. Jamshidi, D. R. Myers, L. Chen, X. A. Fu, M. Mehregany, M. B. J. Wijesundara, and A. P. Pisano, IEEE Sens. J. **7**, 568 (2007).
[44]S. Ghaffari, S. A. Chandorkar, S. Wang, E. J. Ng, C. H. Ahn, V. Hong, Y. Yang, and T. W. Kenny, Sci. Rep. **3**, 3244 (2013).
[45]A. Boisen, S. Dohn, S. S. Keller, S. Schmid, and M. Tenje, Rep. Prog. Phys. **74**(3), 036101 (2011).
[46]R. A. Barton, B. Ilic, S. S. Verbridge, B. R. Cipriany, J. M. Parpia, and H. G. Craighead, Nano Lett. **10**(6), 2058 (2010).
[47]R. Lifshitz and M. L. Roukes, Phys. Rev. B: Condens. Matter **61**(8), 5600 (2000).
[48]B. Chouvion, S. McWilliam, A. A. Popov, and C. H. J. Fox, Proc. Inst. Mech. Eng. C J. Mech. **226**(1), 283 (2012).
[49]Y. Jimbo and K. Itao, J. Horol. Inst. Jpn. **47**, 1 (1968).
[50]M. C. Cross and R. Lifshitz, Phys. Rev. B: Condens. Matter **64**(8), 085324 (2001).
[51]D. M. Photiadis and J. A. Judge, Appl. Phys. Lett. **85**(3), 482 (2004).
[52]X. L. Feng, C. A. Zorman, M. Mehregany, and M. L. Roukes, Solid-State Sensor, Actuator and Microsystems Workshop, 86 (2006).
[53]Z. Hao, A. Erbil, and F. Ayazi, Sens. Actuators, A **109**(1), 156 (2003).
[54]S. Schmid and C. Hierold, J. Appl. Phys. **104**(9), 093516 (2008).
[55]S. Schmid, K. D. Jensen, K. H. Nielsen, and A. Boisen, Phys. Rev. B: Condens. Matter **84**(16), 165307 (2011).
[56]S. Schmid, B. Malm, and A. Boisen, in *Proceedings of the 2011 IEEE 24th International Conference on Micro Electro Mechanical Systems (MEMS)* (2011), p. 481.
[57]H. Yamaguchi, K. Kato, Y. Nakai, K. Onomitsu, S. Warisawa, and S. Ishihara, Appl. Phys. Lett. **92**(25), 251913 (2008).
[58]Y. J. Yi, Y. D. Kim, J. H. Bak, S. R. Lee, K. Heo, S. Hong, K. Char, and Y. D. Park, Curr. Appl. Phys. **11**(3), 746 (2011).
[59]Y. J. Chang, J. M. Gray, A. Imtiaz, D. Seghete, T. M. Wallis, S. M. George, P. Kabos, C. T. Rogers, and V. M. Bright, Sens. Actuators, A **154**(2), 229 (2009).
[60]S. S. Verbridge, D. F. Shapiro, H. G. Craighead, and J. M. Parpia, Nano Lett. **7**(6), 1728 (2007).
[61]H. Ashiba, R. Kometani, S. Warisawa, and S. Ishihara, J. Vac. Sci. Technol., B **30**(6), 06FD03 (2012).
[62]L. Wang, S. Dimitrijev, J. Han, P. Tanner, A. Iacopi, and L. Hold, J. Cryst. Growth **329**, 67 (2011).
[63]S. Singh, J. R. Potopowicz, L. G. Van Uitert, and S. H. Wemple, Appl. Phys. Lett. **19**(3), 53 (1971).
[64]F. Iacopi, G. Walker, L. Wang, L. Malesys, S. Ma, B. V. Cunning, and A. Iacopi, Appl. Phys. Lett. **102**(1), 011908 (2013).
[65]F. Iacopi, R. E. Brock, A. Iacopi, L. Hold, and R. H. Dauskardt, Acta Mater. **61**(17), 6533 (2013).
[66]N. Mishra, L. Hold, A. Iacopi, B. Gupta, N. Motta, and F. Iacopi, J. Appl. Phys. **115**(20), 203501 (2014).
[67]H. Yao, L. Ouyang, and W. Y. Ching, J. Am. Ceram. Soc. **90**(10), 3194 (2007).
[68]K. P. Zetie, S. F. Adams, and R. M. Tocknell, Phys. Educ. **35**(1), 46 (2000).

[69]K. Y. Yasumura, T. D. Stowe, E. M. Chow, T. Pfafman, T. W. Kenny, B. C. Stipe, and D. Rugar, J. Microelectromech. Syst. **9**(1), 117 (2000).
[70]S. Joshi, S. Hung, and S. Vengallatore, EPJ Tech. Instrum. **1**(1), 5 (2014).
[71]V. Hatty, H. Kahn, J. Trevino, C. A. Zorman, M. Mehregany, R. Ballarini, and A. H. Heuer, J. Appl. Phys. **99**(1), 013517 (2006).
[72]X. Li, B. Bhushan, K. Takashima, Ch. W. Baek, and Y. K. Kim, Ultramicroscopy **97**(1), 481 (2003).
[73]H. Kahn, N. Tayebi, R. Ballarini, R. L. Mullen, and A. H. Heuer, Mater. Res. Soc. Symp. **605**, 25 (1999).
[74]A. R. Kermany and F. Iacopi, J. Appl. Phys. **118**(15), 155304 (2015).
[75]W. E. Newell, Science **161**(3848), 1320 (1968).
[76]S. Bianco, M. Cocuzza, S. Ferrero, E. Giuri, G. Piacenza, C. F. Pirri, A. Ricci, L. Scaltrito, D. Bich, and A. Merialdo, J. Vac. Sci. Technol., B **24**(4), 1803 (2006).
[77]P. Li and R. Hu, Microfluid. Nanofluid. **3**(6), 715 (2007).